Three-Phase Isolated High-Power-Factor Rectifier Using Soft-Switched Two-Switch Forward Converter

Yungtaek Jang, David L. Dillman, and Milan M. Jovanović
Power Electronics Laboratory
Delta Products Corporation
P.O. Box 12173, 5101 Davis Drive
Research Triangle Park, NC 27709

***Abstract* — A three-phase, high-power-factor (HPF), soft-switched isolated rectifier is introduced. The proposed circuit employs a discontinuous-voltage-mode (DVM) resonant input rectifier followed by a two-switch forward converter. In addition to achieving HPF rectification, the circuit also offers soft switching of the forward converter switches. The operation and performance of the proposed topology were verified on a 3-kW prototype operating from a three-phase line-to-line voltage of 220 V ± 10%. The experimental results show that the input-current-shaping using the proposed rectifier can be performed with a THD less than 6% over the entire line range and in the load range from full load down to less than 10% of full load. The measured efficiency of the experimental prototype at full load and nominal line was approximately 90%.**

I. Introduction

A three-phase six-switch rectifier followed by an isolated dc-dc converter is typically used in three-phase applications that require high-power-factor (HPF) and galvanic isolation between the input and output [1]–[2]. While this approach offers excellent performance, its major drawback is a relatively high cost due to the high number of switches and complex control that is required to achieve a low input-current harmonic rectification. In cost sensitive applications, circuits with a fewer number of switches and simpler control are preferred.

In the past, several non-isolated three-phase single-switch HPF rectifiers were introduced [2]-[10]. Generally, these single-switch circuits either employ a discontinuous-current-mode (DCM) pulse-width-modulation (PWM) boost rectifier topology [4]-[8], or multi-resonant buck topology [9]-[10]. Whereas the boost rectifier implementations offer a low component count and exhibit high efficiencies, the single-switch multi-resonant non-isolated buck rectifier seem more attractive at high power levels because it exhibits a low THD with continuous input and output currents.

The major drawback of the multi-resonant buck converter rectifier is the voltage stress on the switching devices. As a result, the use of this circuit has been limited to applications with a relatively low line voltage, specifically, to rms line-to-line voltages 380 V and below [10].

In this paper, the multi-resonant HPF rectifier combined with two-switch forward converter topology is introduced. Because the switch voltage in the two-switch forward converter is clamped, this topology exhibits minimal voltage stress across semiconductor switches. For example, for this converter operating from a 220-V ±10% three-phase line, the switch voltage stress is limited to less than 700 V. In addition, the converter offers zero-current switching (ZCS) of the switches, which is the preferred operating mode for IGBT devices. Because all rectifiers operate with zero-voltage turn off, the proposed converter exhibits excellent electromagnetic compatibility (EMC) performance. It should also be noted that since the proposed three-phase HPF front end provides galvanic isolation, a downstream regulator could be a simple non-isolated buck converter.

Finally, since in this variable-frequency controlled HPF isolated rectifier the output power is directly proportional to the switching frequency, the practical minimum switching frequency imposes a lower limit on the output power variation at a given input voltage. A technique that significantly reduces the switching frequency range over the entire input and load range is also described in this paper.

II. 3-ϕ Isolated HPF Multi-Resonant ZCS Two-Switch Forward Rectifier

A. *Principle of Operation*

The circuit diagram of the proposed 3-kW, isolated, HPF, multi-resonant, ZCS two-switch forward rectifier is shown in Fig.1. The primary side consists of input filter inductors L_A, L_B, and L_C, input side resonant capacitors C_1-C_3, input

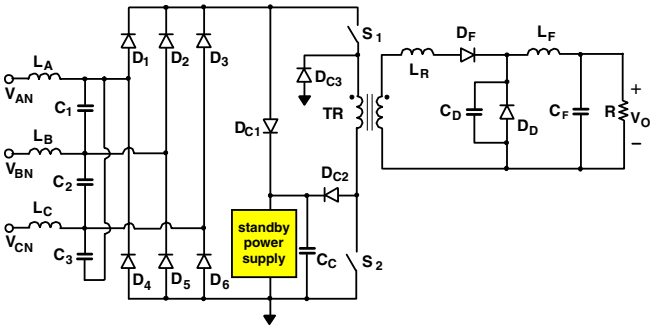

Fig. 1. Proposed isolated three-phase HPF multi-resonant rectifiers employing two-switch forward converter.

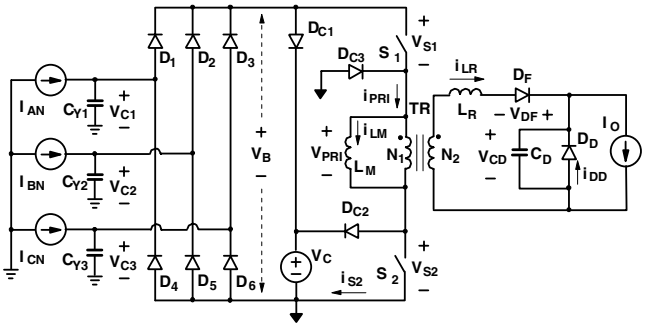

Fig. 2. Simplified circuit diagram of proposed converter with reference directions of voltages and currents.

rectifiers D_1 through D_6, switches S_1 and S_2, and the primary winding of transformer TR. It should be noted that switch voltages are clamped by clamp diodes D_{C1}-D_{C3} and clamp capacitor C_C. The voltage across clamp capacitor C_C is utilized as both the transformer reset voltage and a dc source for the housekeeping power supply.

The output side of the circuit consists of the secondary winding of transformer TR, resonant inductor L_R, secondary-side resonant capacitor C_D, forward diode D_F, output rectifier D_D, and output filter L_F with C_F connected across load R_L.

To facilitate the explanation of the circuit operation, Fig. 2 shows a simplified circuit diagram of the circuit in Fig. 1. In the simplified circuit, Δ-connected input side resonant capacitors C_1-C_3 in Fig. 1 are converted to a Y-connection, which is more convenient to describe the operation. The Y-connected input side resonant capacitors are denoted as C_{Y1}, C_{Y2}, and C_{Y3} as shown in Fig. 2. Moreover, clamp capacitor C_C is modeled by voltage source V_C, assuming that the value of capacitor C_C is large enough that the voltage ripples across the capacitor are small compared to its dc voltage. Input filter inductors L_A, L_B, and L_C are modeled by current sources I_{AN}, I_{BN}, and I_{CN}, respectively. Also, output filter inductor L_F is modeled by current source I_O. Because the inductance of the input and output filter inductors are large, the current ripples in the inductors are small compared to their dc or line frequency currents.

In addition, isolation transformer TR is modeled by magnetizing inductance L_M and an ideal transformer with turns ratio $n=N_1/N_2$, where N_1 is the number of turns for the primary winding and N_2 is the number of turns for the secondary winding. The leakage inductance of transformer TR is neglected in the model since resonant inductor L_R, whose inductance is much larger than the leakage inductance, is connected in series. Finally in this analysis it is also assumed that all semiconductor components have zero impedance in the on state and infinite impedance in the off state.

To further facilitate the analysis of operation, Fig. 3 shows the topological stages of the circuit in Fig. 1 during a switching cycle, whereas Fig. 4 shows its key waveforms. It

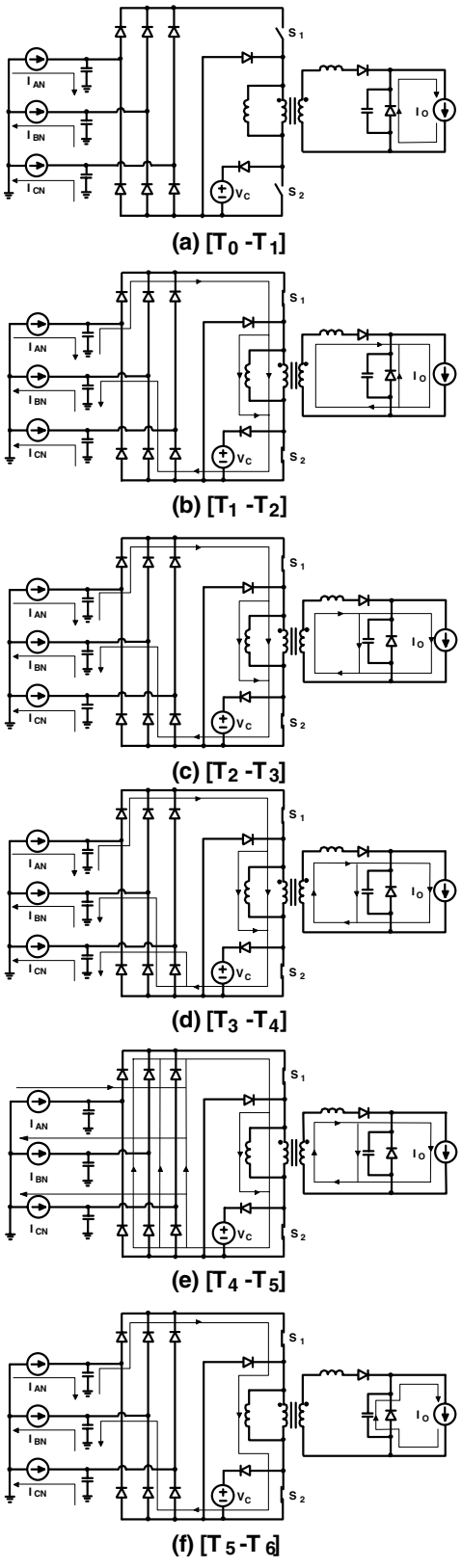

Fig. 3(a)-(f). Topological stages of proposed circuit.

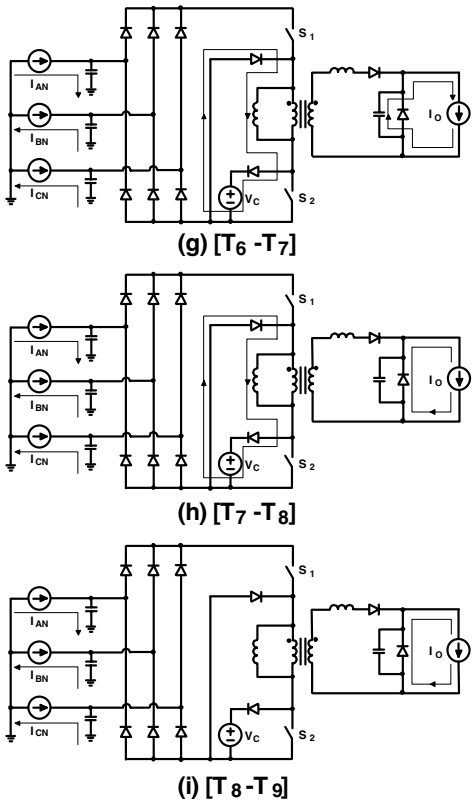

Fig. 3(g)-(i). Topological stages of proposed circuit.

should be noted that the operation shown in Figs. 3 and 4 is within the period when I_{AN}>-I_{BN}>-I_{CN}. The reference directions of currents and voltages plotted in Fig. 4 are shown in Fig. 2.

As can be seen from the timing diagram of the control signals for switches S_1 and S_2 shown in Fig. 4, switches S_1 and S_2 of the proposed circuit are simultaneously turned on and off. It should be noted that switch on-time T_{ON} is constant, whereas, switch off-time T_{OFF} is modulated by the control circuit, leading to a variable switching frequency. During the time interval when switches S_1 and S_2 are open, input currents I_{AN}, I_{BN}, and I_{CN} flow through input resonant capacitors C_{Y1}-C_{Y3}, respectively, as shown in Fig. 3(a). Assuming that at $t=T_0$, transformer TR is completely reset, *i.e.*, magnetizing current $i_{LM}(t=T_0)=0$, no other current is flowing in the circuit during the time interval from $t=T_0$ until switches S_1 and S_2 are turned on at $t=T_1$. Since input currents I_{AN}, I_{BN}, and I_{CN} are constant, the voltages across input resonant capacitors C_{Y1}-C_{Y3} are linearly changed during the $[T_0 - T_1]$ interval, as shown in Fig. 4. The slopes of the voltage variations are as follows,

$$\frac{dV_{C1}}{dt}=\frac{I_{AN}}{C_{Y1}},\quad \frac{dV_{C2}}{dt}=\frac{I_{BN}}{C_{Y2}},\quad \text{and}\quad \frac{dV_{C3}}{dt}=\frac{I_{CN}}{C_{Y3}}. \quad (1)$$

It should be noted that the peak voltages of input resonant capacitors C_{Y1}-C_{Y3} at $t=T_1$ are proportional to input currents I_{AN}, I_{BN}, and I_{CN}. Because input resonant capacitors C_{Y1}-C_{Y3} operate very close to the continuous/discontinuous-voltage-mode boundary (CVM/DVM), their average voltages are proportional to input currents I_{AN}, I_{BN}, and I_{CN}. Since the average voltage of each input resonant capacitor is equal to the phase input voltage, the average voltage across input inductors $L_{A\text{-}C}$ is proportional to the input voltage. As a result, the average inductor current is proportional to the input current and a HPF is achieved.

After switches S_1 and S_2 are closed at $t=T_1$, input resonant capacitors C_{Y1} and C_{Y2} start to resonate with resonant inductor L_R through transformer TR as shown in Fig. 3(b). This period ends at $t=T_2$ when the current of resonant inductor L_R reaches output current I_O. During the $[T_1 - T_3]$ interval, input resonant capacitors C_{Y1} and C_{Y2} are discharged by the resonance while input resonant capacitors C_{Y3} is still linearly charged by input current I_{CN} because diode D_6 is

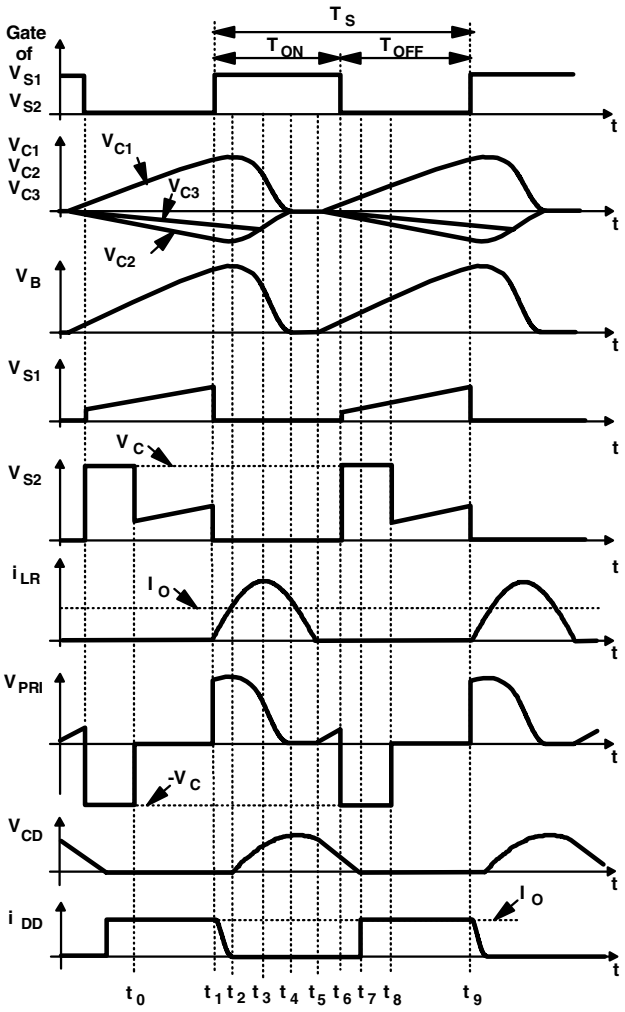

Fig. 4. Key waveforms of proposed circuit.

reverse biased. When capacitor voltage V_{C2} reaches voltage V_{C3} at t=T_3, as shown in Fig. 4, input resonant capacitor C_{Y3} also resonates with resonant inductor L_R, as shown Fig. 3(d). Voltage V_B across the dc side of the input bridge rectifier is the difference between resonant capacitor voltages V_{C1} and V_{C2}, as shown in Fig. 4. After input resonant capacitors C_{Y1}-C_{Y3} are completely discharged at t=T_4, resonant inductor current flows through input bridge diodes D_1-D_6, as shown in Fig. 3(e). When the current of resonant inductor L_R reaches zero at t=T_5, forward diode D_F becomes reverse biased. After t=T_5, small magnetizing current i_{LM} flows through input bridge diodes D_1 and D_5 while the majority of input currents I_{AN}, I_{BN}, and I_{CN} begins charging input resonant capacitors C_{Y1}-C_{Y3}, as shown in Fig. 3(f).

At t=T_6, switches S_1 and S_2 are simultaneously open so that the magnetizing current flows through clamp diodes D_{C2} and D_{C3} and starts to reset transformer TR by clamp voltage V_C, as shown in Fig. 3(g). During the [T_6 – T_7] interval, switch voltage V_{S2} is equal to clamp voltage V_C because clamp diode D_{C2} conducts. It should be noted that switches S_1 and S_2 are turned off when their current is only magnetizing current i_{LM}, which is a negligible amount compared to the resonant current. During the [T_5 – T_7] interval, output side resonant capacitor C_D delivers output current I_O, hence its voltage linearly decreases as shown in Fig. 4. When the voltage of resonant capacitor C_D reaches zero at t=T_7, output diode D_D is forward biased and delivers output current I_O. Transformer TR is completely reset at t=T_8, as illustrated in Fig. 4. The voltages across input resonant capacitors C_{Y1}-C_{Y3} are linearly charged during the [T_5 – T_9] interval, as shown in Fig. 4. The next switching cycle is initiated at t=T_9 when switches S_1 and S_2 are turned on again.

B. Normalized Control Characteristics

To simplify the three-phase input and single-ended output circuit shown in Fig. 2, one operating point at the time π/2 of the angular line frequency is chosen as described in [9]. At this moment, phase voltage V_{AN} is at its peak value, whereas phase voltages V_{BN} and V_{CN} are both negative and equal in magnitude to one-half of V_{AN}. The simplified single input single output circuit model is derived, as shown in Fig. 5. Diodes D_1 and D_2 of Fig. 5 represent the three phase input bridge diodes. The relations between the three phase input circuit and normalized quantities are described approximately by:

(a) $C_X = C_Y \times 2/3$, where resonant capacitors C_{Y1}-C_{Y3} have the same values and are represented as C_Y,

(b) I_g = peak phase current $I_{AN\text{-}PEAK}$,

(c) V_g = 3/2 times peak phase voltage $V_{AN\text{-}PEAK}$,

(d) input power $P_{IN} = V_g \times I_g = 3/2 \times (V_{AN\text{-}PEAK} \times I_{AN\text{-}PEAK})$.

The normalizing base quantities nV_O, I_O/n, R_O, and f_O are defined as:

nV_O — base voltage,

$I_B = nV_O/R_O$ — base current,

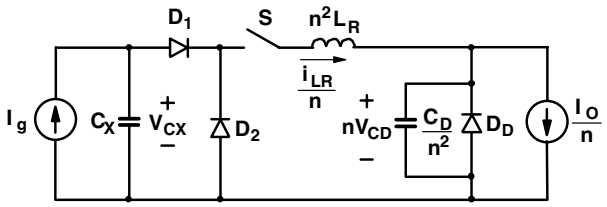

Fig. 5. Simplified single input and single output circuit model of proposed circuit in Fig. 3.

$R_O = \sqrt{n^2 L_R / C_X}$ — characteristic impedance,

$f_O = 1\Big/\left(2\pi\sqrt{n^2 L_R C_X}\right)$ — base frequency,

where V_O is the output voltage of the rectifier. Therefore, the normalized values of the input and output quantities are:

normalized input voltage $M_g = V_g/(nV_O)$,

normalized input current $J_g = I_g R_O/(nV_O)$,

normalized output current $J_O = I_O R_O/(n^2 V_O) = M_g J_g$.

Figure 6 shows the input characteristic of the converter, *i.e.*, normalized input current J_g vs. normalized input voltage M_g, for normalized switching frequency $F = f_S/f_O$ as a parameter, as derived in [9] and [10]. Figure 6 is indispensable in determining the converter's steady-state operating point and design parameters. The shaded area in Fig. 6 is the operating area for the experimental 3 kW converter.

C. Resonant Component Design

A 3-kW HPF rectifier is required to deliver an isolated 400 V_{DC} output from a 3-ϕ 220 $V_{L\text{-}L}$ ±10% input. Because the input line-to-line voltage is 220 V, effective input voltage $V_{g\text{-}NOM} = \frac{3}{2} \times V_{AN-PEAK} = \frac{3}{2} \times \frac{220\sqrt{2}}{\sqrt{3}} =$ 269.4V, therefore, normalized nominal input voltage $M_{g(NOM)} = V_{g\text{-}NOM}/(nV_O)$= 269.4/200 = 1.34 when turns ratio n=0.5. From Fig. 6, normalized nominal input current $J_{g(NOM)}$ is chosen to be 0.72 for the maximum output power of 3 kW so that the selection of $J_{g(MAX)}$ =0.8 at low line allows for over a 30% margin from the zero-current-switching (ZCS) boundary ($J_{g(ZCS)} \approx 1.2$), ensuring ZCS over the entire input-voltage range including some transient condition. Since at maximum output power $M_{g(NOM)}$ = 1.34 and $J_{g(NOM)}$ = 0.72, normalized full-load frequency $F_{FL\text{-}NOM}$ is determined as $F_{FL\text{-}NOM}$ = 0.89, as shown in Fig. 6. Furthermore, because output current $I_O = P_O/V_O$ = 7.5 A, characteristic impedance is $R_O = M_{g(NOM)} J_{g(NOM)} n^2 V_O/I_O$ = 9.5 Ω. If the switching frequency at full load and nominal line is chosen to be $f_{S(NOM)}$ = 70 kHz, then resonant frequency f_O can be calculated as $f_O = f_{S(NOM)}/F_{FL}$ = 70/0.92 = 76 kHz. It should be noted that the maximum switching frequency is approximately 75 kHz at full load and low line.

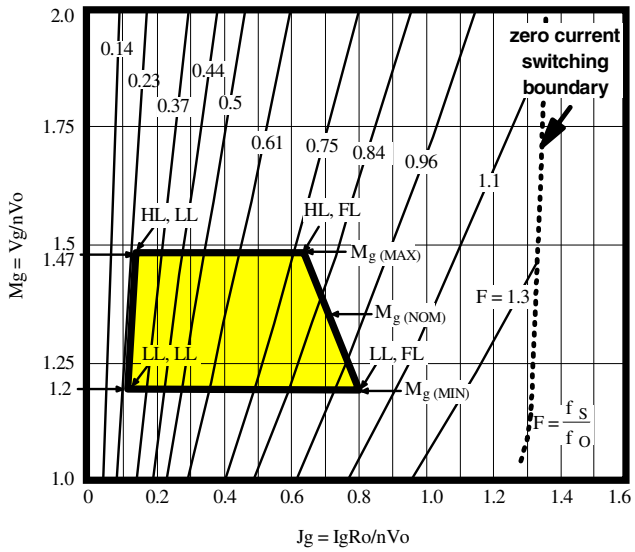

Fig. 6. The normalized input characteristic of proposed circuit in Fig. 6. The normalized frequency F is defined as the ratio of the switching frequency f_S and the resonant frequency f_O. The shaded area is the operating area for the experimental 3 kW converter.

The operating region for this design is indicated as the shaded area in Fig. 6. Three salient points which define the operating region are high-line full-load (HL, FL), nominal-line full-load (NL, FL), low-line full-load (LL, FL). The maximum normalized input voltage $M_{g(MAX)}$ is 1.47 at input-voltage of 220 V_{L-L} + 10% and the minimum normalized input voltage $M_{g(MIN)}$ is 1.2 at an input-voltage of 220 V_{L-L} - 10%. The calculated effective capacitance C_X is $C_x = 1/(2\pi R_O f_O)$ = 220 nF, whereas the resonant inductance is $L_R = R_O/(2\pi f_O n^2)$ = 80 uH. Therefore, input-side Δ-connected resonant capacitors C_1-C_3 = C_X /2 = 110 nF and the value of output-side resonant capacitor C_D is chosen to be $C_X \times n^2 = C_d$ = 55 nF. This choice leads to a good compromise between low voltage stress and low input-current harmonics.

Due to the wide input-voltage and load ranges, the closed-loop control of the prototype rectifier is implemented by a combination of variable- and constant-frequency control. The circuit frequency is controlled in the range between full load and light load. In this power range the switching frequency varies from 75 kHz at full load to 20 kHz at light load. When the switching frequency falls to 20 kHz, the constant frequency PWM control takes over to regulate the output voltage without further decreasing the switching frequency. When the constant-frequency PWM control is active, the switch operates with "hard" switching. To minimize switching loss during the PWM operation, the switch current should be minimized. This can be achieved by selecting input inductors L_A-L_C to form a 20-kHz resonant tank circuit with input resonant capacitors C_1-C_3. At the moment when switches S_1 and S_2 are turned off, the currents of input inductors L_A-L_C begin to charge input resonant capacitors C_1-C_3 in resonant fashion. Because the resonant frequency and the switching frequency are nearly the same, the stored energy in input resonant capacitors C_1-C_3 was already decreased to near zero by the resonant currents of input inductors L_A-L_C at the moment when switches S_1 and S_2 are turned on again. As a result, because there is no energy in input resonant capacitors C_1-C_3 to resonate with resonant inductor L_R, the switch current decreases dramatically at 20-kHz operation, hence switching losses are minimized even when operating with hard-switching PWM operation. The value of input inductors L_A-L_C is selected to be approximately 300 μH to form a 20-kHz resonant tank circuit with input resonant capacitors C_1-C_3.

Since during operating conditions when the constant-frequency PWM control or line and load transients are active and the switches operate with "hard" switching, the passive clamp circuit, shown in Fig. 1, is used to prevent any voltage overshoot. In fact, if the switch is turned off while a certain amount of current is flowing through it, the switch current is diverted through diodes D_{C1}-D_{C3} and clamping capacitor C_C. Because the output power is low in the constant-frequency PWM control mode, the clamping circuit operates with negligible losses.

III. Experimental Results

The performance of the proposed isolated, 3-phase, HPF, resonant, two-switch forward rectifier topology was verified on a 3-kW experimental prototype operating at 20 kHz to 75-kHz switching frequency and providing 400-V dc output voltage.

A. Component Selection

To reduce the conduction loss and temperature of the switches, two IGBTs were connected in parallel for S_1 and S_2 (Fairchild, FGL60N100, V_{CES} = 1000 V, I_{C90} = 60 A). Because the switches are punch-through (PT) type IGBTs that have a negative thermal feedback characteristic, the parallel operation of the IGBT provides much better thermal performance than that of the single IGBT operation.

A high voltage diode from Fairchild (FFAF10U170S, V_{RRM} = 1700 V, I_{FAVM} = 10 A) was employed as secondary side forward diode D_F. Because the maximum voltage stress across input bridge diodes D_1-D_6 and output diode D_D is approximately 700 V, high voltage diodes from Fairchild (FFAF10U170S, V_{RRM} = 1000 V, I_{FAVM} = 30 A) were employed.

High voltage polypropylene capacitors with values of 100 nF (CDE, 940C20P1K, 2kV, 8.3 A_{RMS}) and 10 nF (CDE, 940C30S1K, 3kV, 2 A_{RMS}) were used in parallel for input-side resonant capacitors C_1-C_3. Two polypropylene capacitors with values of 47 nF (CDE, 940C20S47K, 2kV, 5.2 A_{RMS}) and 10 nF were connected in parallel and used for output-side resonant capacitor C_D. The total values of the input- and output-side resonant capacitors were 110 nF and 57 nF, respectively.

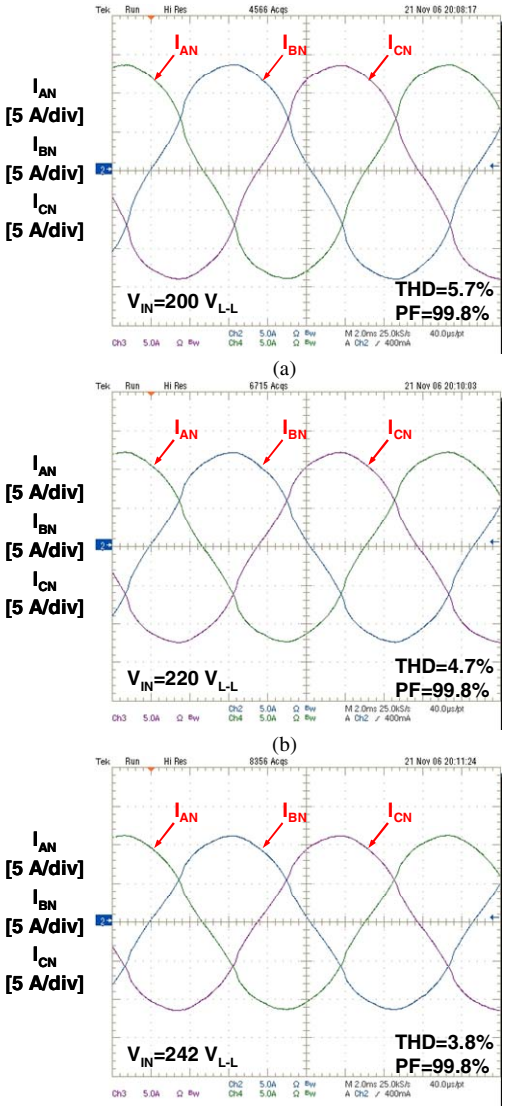

Fig. 7. Measured three-phase current waveforms of experimental prototype at P_O=3 kW and (a) V_{IN}=200 $V_{L\text{-}L}$, (b) V_{IN}=220 $V_{L\text{-}L}$, (c) V_{IN}=242 $V_{L\text{-}L}$, . Time base: 2 ms/div.

The desired inductance of input filter inductors L_A, L_B, and L_C was 300 µH for each phase. Two high-flux toroidal cores (Arnold, HF488075-2) were used in parallel to reduce the flux density and number of turns of the winding. A magnet wire (45 turns, AWG# 13) was used as the inductor winding.

The inductance of resonant inductor L_R was 80 µH to obtain the desired resonant frequency of 76 kHz. A set of ferrite EE cores (ETD44/21-3F3, air gap=6 mm) was used. Litz wire (435 strands, AWG# 40, 45 turns) was used to reduce the proximity effect of the winding.

The inductance of output filter inductor L_F was 900 µH. A set of ferrite EE cores (E65/32/27-3C94, air gap=40 mils) was used. A solid magnet wire (50 turns, AWG# 12) was used because the proximity effect in the output filter inductor was negligible.

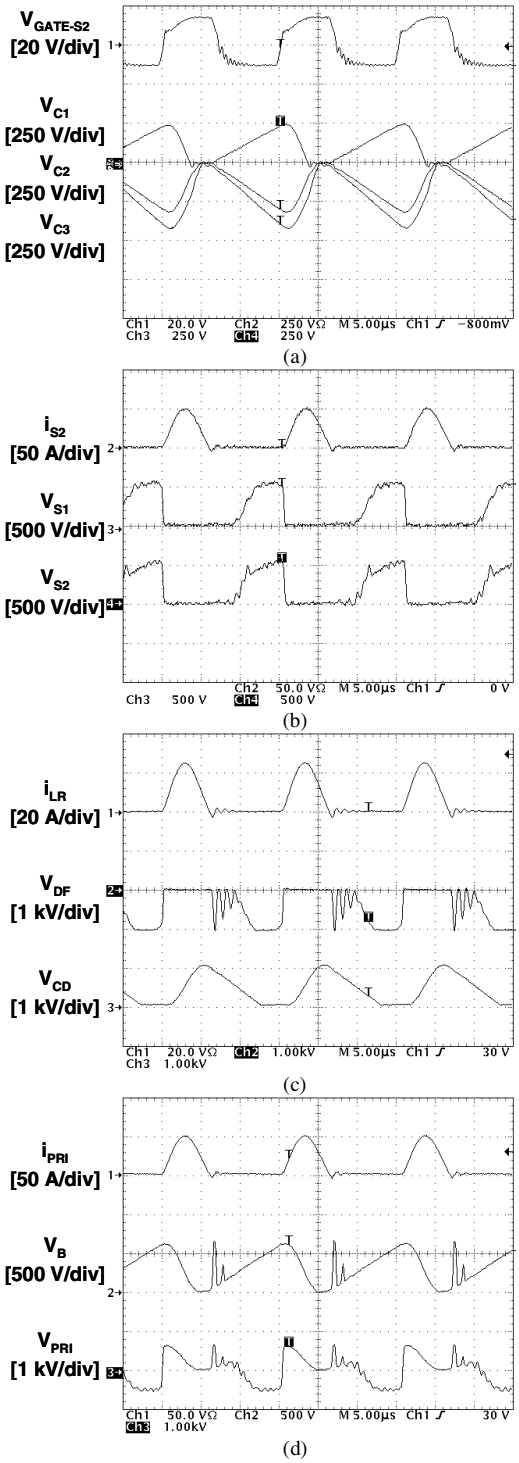

Fig. 8. Measured waveforms of experimental prototype at V_{IN}=220 $V_{L\text{-}L}$, V_O=400 V_{DC}, and P_O=3 kW. Time base: 5 µs/div.

Finally, two sets of EE cores (E80/38/20-3C94, air gap=1 mil) were used in parallel to construct isolation transformer TR. Two Litz wires (435 strands, AWG# 40, 22 turns) connected in parallel were used as the primary winding and a

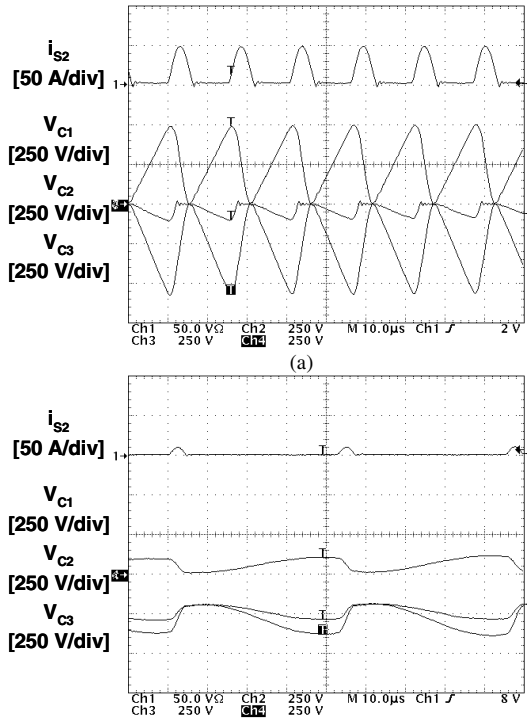

Fig. 9. Measured waveforms of experimental prototype delivering (a) P_O=3 kW at f_S=67 kHz and (b) P_O=200W at f_S=23 kHz and V_{IN}=220 $V_{L\text{-}L}$. Time base: 10 µs/div.

Litz wire (435 strands, AWG# 40, 44 turns) was used as the secondary winding of the transformer.

B. Measured Results

Figures 7(a) – 7(c) show the measured waveforms of the input line current delivering 3 kW at prototype rectifier's three input voltages: V_{IN} = 200 V, 220 V, and 242 V. Results demonstrate total-harmonic-distortion (THD) of less than 6% at full output power and less than 5% THD at 50% output power. The rectifier efficiency is approximately 91% at 50% load and approximately 90% at full load and nominal line.

Figures 8(a)-8(d) show the measured waveforms of key components. All the measured waveforms in Fig. 8 have the same time scale and aligned to the equal trigger moment. Figure 8(a) shows the measured gate-to-source voltage of switch S_2 which is identical to the gate-to-source voltage of switch S_1 and the measured voltage waveforms of input resonant capacitors C_1-C_3. Figure 8(b) shows the measured current waveform of switch S_2 and the drain-to-source voltage waveforms of switches S_1 and S_2. As shown in Fig. 8(b), the measured voltage stresses of the switches are well below the employed IGBT's nominal voltage rating (1 kV). Figure 8(c) shows the measured current waveform of resonant inductor L_R, voltage waveforms across forward diode D_F and output resonant capacitor C_D. Figure 8(d) shows the current and voltage waveforms of primary winding of transformer TR and voltage waveform of V_B. As shown in Fig. 8(c), the voltage across forward diode D_F is well clamped to 1 kV, which is also well below the device rating of 1.7 kV.

Finally, Fig. 9 shows the measured current waveforms of switch S_2 and the voltage waveforms of input resonant capacitors C_1-C_3 at full load with switching frequency of 67 kHz and light load with switching frequency of 20 kHz. The switch current decreases dramatically at 20-kHz operation.

IV. SUMMARY

A three-phase soft-switched rectifier that provides galvanic isolation and automatically achieves HPF by employing a DVM resonant input circuit and a two-switch forward converter has been introduced. The performance of the proposed topology was verified on a 3-kW prototype operating from a three-phase input voltage of 220 $V_{L\text{-}L}$ ± 10%. The experimental results show that the input-current-shaping using the proposed rectifier can be performed with less than 6% THD over both the entire line range and full load to less than 10% load range. The measured efficiency at full load and nominal line is approximately 90%.

REFERENCES

[1] A. R. Prasad, P. D. Ziogas and S. Manias, "An active power factor correction technique for three-phase diode rectifiers," *IEEE Power Electronics Specialists Conf. (PESC) Record*, pp. 58 – 66, 1989.

[2] H. Mao, D. Boroyevich, A. Ravindra, and F. C. Lee, "Analysis and Design of High Frequency Three-phase Boost Rectifiers," *IEEE Applied Power Electronics Conf. (APEC) Record*, pp. 538 – 544, 1996.

[3] E. H. Ismail and R. W. Erickson, "A single transistor three-phase resonant switch for high quality rectification," *IEEE Power Electronics Specialists Conf. (PESC) Record*, pp. 1341 – 1351, 1992.

[4] L. Simonetti, J. Sebastian, and J. Uceda, "Single-Switch Three-Phase Power Factor Under Variable Switching Frequency and Discontinuous Input Current," *IEEE Power Electronics Specialists Conf. (PESC) Record*, pp. 657 - 662, 1993.

[5] J. W. Kolar, H. Ertl, and F. C. Zach, "Space Vector-Based Analytical Analysis of the Input Current Distortion of A Three-Phase Discontinuous-Mode Boost Rectifier System," *IEEE Power Electronics Specialists Conf. (PESC) Record*, pp. 696 - 703, 1993.

[6] Q. Huang and F. C. Lee, "Harmonic Reduction in A Single-Switch, Three-Phase Boost Rectifier with High Order Harmonic Injected PWM," *IEEE Power Electronics Specialists Conf. (PESC) Record*, pp. 1266 - 1271, 1996.

[7] J. Sun, N. Frohleke, and H. Grotstollen, "Harmonic Reduction Techniques for Single-Switch Three-Phase Boost Rectifiers," *Conference Record of the 1996 IEEE Industry Applications Society Annual Meeting*, pp. 1225 - 1232, 1996.

[8] Y. Jang and M. M. Jovanović, "A New Input-Voltage Feedforward Harmonic-Injection Technique with Nonlinear Gain Control for Single-Switch, Three-Phase DCM Boost Rectifier," *IEEE Transactions on Power Electronics, Vol. 15, no. 2*, pp. 268-277, March 2000.

[9] Y. Jang and R. W. Erickson, "New single-switch three-phase high power factor rectifiers using multi-resonant zero current switching," *IEEE Applied Power Electronics Conf. (APEC) Record*, pp. 711 – 717, 1994.

[10] Y. Jang, M. M. Jovanović, "Design Considerations and Performance Evaluation of a 6-kW, Single-Switch, Three-Phase, High-Power-Factor, Multi-Resonant, Zero-Current-Switching Buck Rectifier," *International Telecommunications Energy Conf. (INTELEC) Record,* pp. 715 - 722, 1997.